

**Design and Characterisation of a Quiet, Low Turbulence  
Open Jet Blow Down Wind Tunnel in ISVR**

**T.P. Chong, P.F. Joseph and P.O.A.L. Davies**

ISVR Technical Report No 322

March 2008



## SCIENTIFIC PUBLICATIONS BY THE ISVR

**Technical Reports** are published to promote timely dissemination of research results by ISVR personnel. This medium permits more detailed presentation than is usually acceptable for scientific journals. Responsibility for both the content and any opinions expressed rests entirely with the author(s).

**Technical Memoranda** are produced to enable the early or preliminary release of information by ISVR personnel where such release is deemed to be appropriate. Information contained in these memoranda may be incomplete, or form part of a continuing programme; this should be borne in mind when using or quoting from these documents.

**Contract Reports** are produced to record the results of scientific work carried out for sponsors, under contract. The ISVR treats these reports as confidential to sponsors and does not make them available for general circulation. Individual sponsors may, however, authorize subsequent release of the material.

### COPYRIGHT NOTICE

(c) ISVR University of Southampton All rights reserved.

ISVR authorises you to view and download the Materials at this Web site ("Site") only for your personal, non-commercial use. This authorization is not a transfer of title in the Materials and copies of the Materials and is subject to the following restrictions: 1) you must retain, on all copies of the Materials downloaded, all copyright and other proprietary notices contained in the Materials; 2) you may not modify the Materials in any way or reproduce or publicly display, perform, or distribute or otherwise use them for any public or commercial purpose; and 3) you must not transfer the Materials to any other person unless you give them notice of, and they agree to accept, the obligations arising under these terms and conditions of use. You agree to abide by all additional restrictions displayed on the Site as it may be updated from time to time. This Site, including all Materials, is protected by worldwide copyright laws and treaty provisions. You agree to comply with all copyright laws worldwide in your use of this Site and to prevent any unauthorised copying of the Materials.

**Design and Characterisation of a Quiet, Low Turbulence  
Open Jet Blow Down Wind Tunnel in ISVR**

by

T P Chong, P F Joseph and P O A L Davies

March 2008

**ISVR**

**TECHNICAL REPORT No. 322**

# Contents

1. Abstract .....	2
2. Introduction .....	3
3. The Open Jet Facility .....	4
4. Design Principle .....	6
5. Layout of the Quiet Open Jet Facility .....	9
5.1. Control Valve .....	10
5.2. Primary Silencer .....	12
5.3. 90 <sup>0</sup> -Curved Diffuser .....	14
5.4. Settling Chamber / Secondary Silencer.....	20
6. Calibration of the Open Jet Wind Tunnel .....	24
6.1 Analysis of Background Noise Levels .....	25
6.2 Analysis of Exit Flow Uniformity and Turbulence Characteristics.....	30
7. Measurements of Aerofoil Trailing Edge Noise .....	31
8. Conclusions .....	32
9. Acknowledgements .....	33
10. Nomenclatures.....	34
11. References .....	35

## 1. Abstract

This technical report presents the design of an open-jet, blow-down wind tunnel that was newly commissioned in the anechoic chamber at the ISVR, University of Southampton, UK. This wind tunnel is intended for the measurement of airfoil trailing edge self-noise but can be extended to other aeroacoustic applications. With the primary objectives of achieving acoustically quiet and low turbulence air jet up to 120m/s through a 150mm x 450mm nozzle, several novel noise and flow control techniques were implemented in the design. Both the acoustical and aerodynamic performances of the open jet wind tunnel were calibrated in detail after its fabrication. It is found that the background noise of the facility is adequately low for a wide range of exit jet velocity. The potential core of the free jet is characterised by a low turbulence level of about 0.1%. A benchmark test by submerging a NACA0012 airfoil with a tripped boundary layer at zero angle of attack into the potential core of the free jet was carried out. It was confirmed that the radiating aerofoil trailing edge self-noise has levels significantly above the rig noise over a wide range of frequencies. The low noise and low turbulence characteristics of this open jet wind tunnel are comparable to the best facilities in the world, and is believed to be the first of its kind in the UK.

## 2. Introduction

Until recently the main source of engine noise from commercial aircraft has been from the jet. With the advance of more effective low-noise engine technologies, such as ultra high bypass ratio engine and lower speed fans, significant reduction of the jet noise was realised. By contrast, due to a relatively poorer understanding on the fan broadband noise, it has become a dominant noise source in modern aero-engine. One of the frequently quoted noise problem that occurs in this area is the noise generated by interaction of the turbulent boundary layer with the trailing edge of the fan blades. In this case the vortical disturbances of the turbulent boundary layer scatter at the sharp trailing edge and transform into acoustic disturbances such as the broadband trailing edge self-noise. Trailing edge self-noise is also a dominant noise generation mechanism on aircraft wings and wind turbines. The ability to predict and characterise the trailing edge self-noise is therefore important for its understanding and mitigation. A number of theoretical and computational models of trailing edge self-noise may be found in the literatures<sup>1-5</sup>. However, experimental studies of trailing edge noise are comparatively scarce<sup>6-8</sup>, most likely due to the numerous difficulties in obtaining accurate trailing edge self-noise measurement. The main difficulty with this measurement is the high levels of background noise such as from the fan most commonly used to generate the air flow, structural vibration noise and noise induced by flow through various components of the test tunnel. These extraneous noises, especially in high Reynolds number experiments, can easily mask the relatively weak broadband trailing edge self-noise.

Essential requirements of an open jet wind tunnel for aeroacoustic measurements are that, most importantly, the trailing edge self-noise should be significantly greater than the background noise (more than 10dB); second, the incoming flow should be of sufficiently low turbulence intensity to eliminate additional noise sources caused by the interaction of the vortical disturbances with the leading edge. One can summarise these requirements into acoustic and aerodynamic aspects of the wind tunnel respectively. It is perhaps reasonable to assume that a wind tunnel with good aerodynamic performance should equally possess good acoustic characteristic<sup>i</sup> and the opposite is sometimes true. A number of high quality aeroacoustic wind tunnels exist in university and research

---

<sup>i</sup> For example, the growths of unsteady and separated flows inside a wind tunnel component as the results of ill-design can always emit flow-induced noise.

organisations that comply with these requirements at low to moderate Reynolds numbers<sup>9-11</sup>. However, the design of a high speed aeroacoustic wind tunnel that matches the operating Reynolds numbers an aircraft turbo-engine inlet fan, typically from  $1-3 \times 10^6$  (based on axial velocities at 30% from the blade root to blade tip respectively) at approach<sup>12</sup>, and yet still retains low background noise and low turbulence intensity is significantly more difficult to achieve.

In April 2004, a research project sponsored by MSTARR DARP was commenced in the Fluid Dynamics and Acoustics Group at ISVR, University of Southampton. The objectives of the project are to build a high speed, quiet and low turbulence open jet blow down wind tunnel and use it to study the aerofoil trailing edge self-noise. To enable accurate farfield noise measurements the jet nozzle is situated in the ISVR's 8m x 8m x 8m anechoic chamber with jet exhaust finally passing through a hole in the wall of the anechoic chamber into an adjoining room.

This technical report presents the design principle of the open jet wind tunnel, with special emphasis on the acoustic and aerodynamic optimisations. Major components such as the silencer, diffuser, settling chamber and nozzle will be described in detail. Calibration results of the facility background noise and the exit jet turbulence levels and flow uniformity will also be included. Finally, a measurement of the trailing edge noise from a symmetric NACA0012 aerofoil in a quiet configuration of zero angle of attack is presented and is shown to be up to 15dB above the background noise level. The low noise and low turbulence characteristics of this open jet wind tunnel are comparable to the best facilities in the world, and it is believed to be the first of its kind in the UK. It is hoped that this report will serve as a technical reference for any works to be conducted, in the future, on this facility.

### 3. The Open Jet Facility

A wind tunnel represents a useful tool for aerodynamic research. Designed for experiment that usually involves scaled-down models, a wind tunnel can be used to simulate flow phenomenon that is otherwise pertinent to full-scale application under controlled environments. To achieve this, a wind tunnel should be capable of operating at high velocity in the test section so as to attain the comparable Reynolds numbers between the smaller scale and full scale applications. It is to this end, that

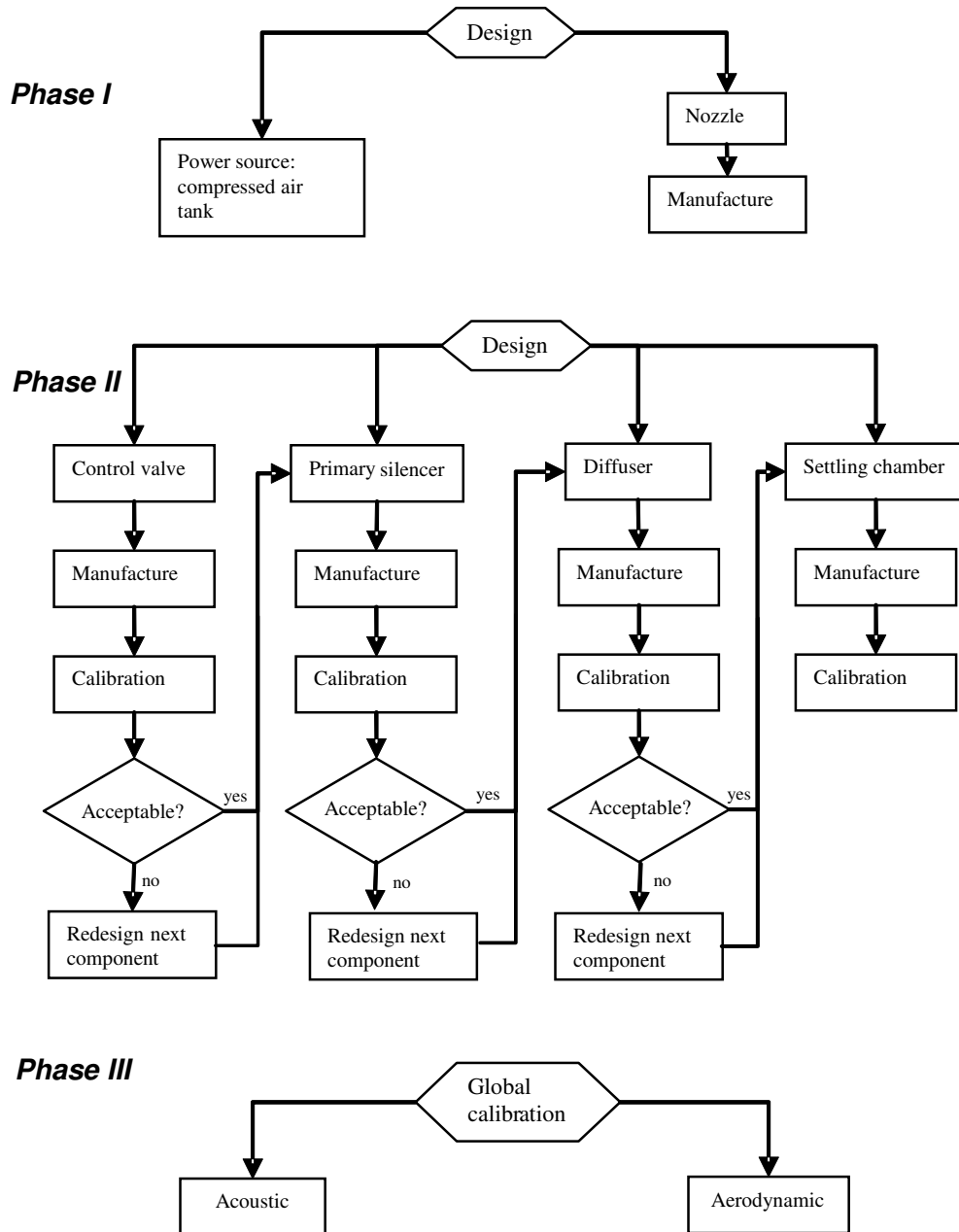


**Fig 1.** Different phases of the open jet wind tunnel design, fabrication and characterisation processes.

the test section of a wind tunnel is usually designed of closed-type because this configuration allows flexible adjustment of the internal pressure distributions. However, in the current study, the farfield broadband noise generated by the interaction of turbulent boundary layer on an aerofoil surface and its trailing edge is the centre of investigation for this study. To measure the radiated noise accurately a

diffuse field is needed. This thereby precludes the practicability of a closed-type test section for the current design.

#### 4. Design Principle

The open jet wind tunnel is designed to fulfil the following acoustic and aerodynamic criteria:

1. Airfoil trailing edge self-noise must be at least 10dB above the facility noise over a wide range of frequencies
2. Maximum Mach number of about 0.3
3. Typical turbulence intensity of less than 0.5%
4. The jet working section is situated in the ISVR's large anechoic chamber for the free field measurement of the self-noise of objects located in the jet
5. The air must be adequately exhausted from the anechoic chamber

As shown in Fig.1 for the wind tunnel designing process, this work was first launched in *Phase I* where the test section was chosen as an open jet type due to the need for making noise measurements in the farfield of objects placed in the air stream. To reproduce the aero-engine operating condition the wind tunnel is designed to deliver a maximum mass flow rate of about 8kg/s. With Mach number of 0.3 this gives the required nozzle exit area as 675cm<sup>2</sup>. Large contraction ratio (*CR*) nozzle is desirable in order to reduce the lateral velocity fluctuations and hence the turbulence level of the exit jet. For such purpose the *CR* is usually taken as 20-25:1, which gives the inlet area of the nozzle between 1.35 – 1.70m<sup>2</sup>.

The next step is to choose, out of two common options, the appropriate power source to run the open jet wind tunnel. The first option is to continuously generate moving air stream by the use of motorised centrifugal blower. The second is to compress and store highly pressurised air in tanks and then release it, in a controllable manner, into the wind tunnel. The centrifugal blower would produce exit jet in a continuous manner – a feature that could potentially be more superior compared to the compressed air option because the latter has only a limited running time. The air stream power needed to run the current application is estimated as 41kW. Since the cumulative total pressure losses caused by the wind tunnel

components and, if any, flow control devices are not negligible, a higher electrical power motor with relatively high fan rpm is required. This may cause undesirable effects such as the elevated fan tonal noise,

mass flow rate (kg/s)	Exit jet speed (m/s)	Running time (s)
2	24	313
4	48	156
6	73	104
8	97	78

**Table 1** Summary of the open jet wind tunnel running time at different mass flow rates and exit jet speeds

temperature irregularities and large swirling flow. Although these adversities are usually straight forward to mitigate, they always come with space and cost penalties. On the other hand, the ISVR in Southampton possesses two large scale compressors that can compress and store air pressure up to 2000kpa in remote reservoirs with a total volume of 30m<sup>3</sup>. It is possible to tap off the compressed air from the reservoirs through steel pipes and run the wind tunnel for a finite time. Table 1 summarises the running times of the open jet wind tunnel at different mass flow rates/jet speeds with the nozzle exit area of (0.15x 0.45)m<sup>2</sup>. By taking into account the already existence of this resource and the likelihood of large pressure losses due to the requirement of adding silencers and flow control devices in the wind tunnel, the compressed air option was finally chosen. The flow rate of the compressed air is regulated by a control valve, and after considering the extraneous mechanical noise generated from the valve and the associated high dynamic pressure, it becomes necessary to attenuate the valve noise by some form of silencing device. This will be discussed in Sections 4 and 5.

For *Phase I*, the “head (compressor)” and “tail (nozzle)” of the open jet wind tunnel had been decided. In *Phase II* the floor space available for accommodating the “in-between” wind tunnel components such as the control valve, silencer, diffuser and settling chamber was surveyed. In order to achieve a good flow quality with low turbulence free jet and minimal flow-induced noise levels, each individual design of the above components was performed simultaneously, but in an iterative manner. In contrary, as shown in Fig. 1, the constructions and installations of the above components were not carried out simultaneously but in sequence starting from the control valve until reaching the settling chamber. An important feature in *Phase II* is that after one component was constructed it will subsequently be calibrated and characterised before continue to build the next component. A key advantage of this approach is that the acoustic or aerodynamic behaviours of the flow when it reaches

a particular component can always be examined first before deciding whether to retain or alter the design of the next components. Finally, the *global* acoustic and aerodynamic (flow leaving the nozzle exit) calibrations of the open jet wind tunnel were performed in *Phase III*.

Apart from attempting to achieve low noise and low turbulence air jet, there are other minor design criteria that should be met:

- (1) Minimum structural vibrations.
- (2) Good ventilation system in the anechoic chamber.
- (3) Easy assembly of the rig.

(1) Minimum structural vibration can be achieved by using thicker plywood skin. In addition to the benefit of structural stability and rigidity, thick tunnel skin is also useful for the attenuation of acoustic transmission through wall. On the other hand, maximum structural deflection due to the uniform internal pressure loading at normal working condition was calculated, based on beam theory, to be not exceeding 2mm for the longest part of the rig. To strengthen the structure, steel flanges are mounted on the tunnel skin at where the maximum deflection occurs.

(2) It was estimated that a maximum mass flow rate of 8kg/s can be constantly injected into the anechoic chamber. For a perfectly sealed chamber (no air leakage), it turns out that once the wind tunnel is switched on, the internal pressure can be increased to about 1.6 bar gauge and each side of the chamber wall has to sustain about  $1 \times 10^7$  N of force after 2 minutes! The ability to vent out the air effectively is therefore paramount to the global design. On the other hand, in order to achieve clean aeroacoustic measurements, minimal residual noise should be generated in the process of air ventilation. Several noise-control options, such as using the screens to slow down the jet speed, deflector to divert the flow path and conical diffuser to collect the exhaust air were considered. Under the principle of achieving low noise ventilation that involves minimal support of materials, a straight forward method is to cut a hole on the anechoic chamber wall that encompassing the air jet where the air is pumped into the adjoining room and eventually leaves the building through the main entrance. This system is extremely effective in terms of air ventilation to avoid excessive internal pressure build up but at the same time keep the flow-structure interaction noise to a minimum.

(3) Like many other wind tunnel designs, a large part of the system consists of pre-tensioned woven wire cloth mesh screens. The screens are mainly used to

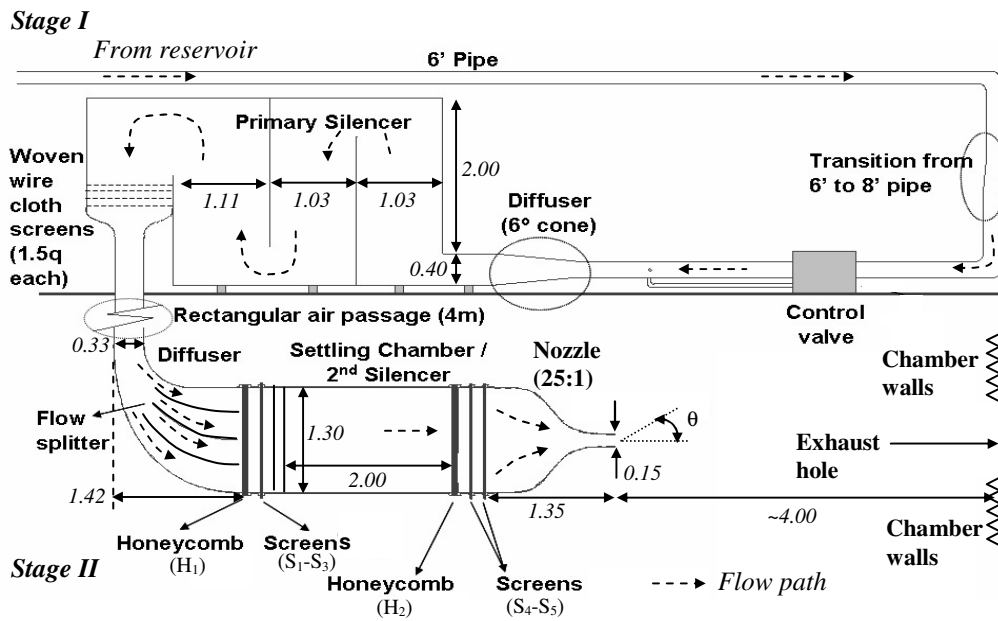


**Fig. 2** Elevation view of the quiet, low turbulence blow down open jet wind tunnel in ISVR. All units in m.

dissipate large scale vortices in the flow. Because most of the screens are finely interconnected, they can easily attract dirt and dust that may present in the flow. A dirty screen is prone to generating vortex shedding, which subsequently increases the fluctuation level in the main flow. Hence, the screens should be cleaned frequently. In view of this, most components of the test rig are joined by bolts/nuts via steel flanges with detachable side wall. This will allow different parts of the rig be separated and joined easily.

## 5. Layout of the Quiet Open Jet Facility

The layout of the quiet open jet wind tunnel is shown in Fig. 2. Air is first pressurised to 2000kPa in tanks upstream of the control valve. The control valve are located in the roof space of the anechoic chamber (*Stage I*), which when opened reduces the downstream air pressure to 200kPa. The air is then expanded in the 8" (20cm) diameter steel pipe through a wide-angle conical diffuser into a 1.3 x 2.4 x 4.1m three-pass silencer. After leaving the silencer the air is accelerated vertically downward to *Stage II* through a 3:1 area ratio 2D nozzle into a 0.33 x 1.3 x 4m duct located next to the wall of the anechoic chamber. The air is then turned by a 90°-curved diffuser and expanded from an inlet area of 0.33 x 1.3m to an outlet area of 1.3 x 1.3m over an axial distance of 1.4m. The straightness and uniformity of the exit air are improved by employing a honeycomb and three fine woven wire mesh

screens before entering a 1.3 x 1.3 x 2m splitter silencer, which also acts to settle the flow. Finally, further flow conditioning is achieved by the use of additional honeycomb and fine woven wire mesh screens before the air accelerates through a 25:1 CR 3D nozzle. The nozzle has a rectangular exit area of 0.15 x 0.45m, which gives an aspect ratio of 3. The resulting maximum Reynolds number based on the hydraulic diameter at the nozzle exit is  $1.5 \times 10^6$ . The nozzle exit is situated at the centre of the anechoic chamber. As shown in Fig. 2, the air jet is finally exhausted through a hole in the wall facing the nozzle exit into a large adjoining room from where the air leaves through doors and windows into the outside. The distance between the nozzle and the exhaust hole is about 4m. The jet was slowed down and diffused inside the adjoining room. The transmission of the flow-structure interaction noise is reduced by the acoustic wedges on the anechoic chamber wall. Hence the excess noise is contained within the adjoining room and will not be picked up inside the anechoic chamber. In the remainder of this section detailed descriptions of the various parts of the open jet wind tunnel, starting from the control valve in the *Stage I*, are presented.

### 5.1. Control Valve

Control valve (also called pressure reducing valve) regulates the flow, the rate, the volume, the pressure or the direction of gases, liquids or slurries in a process system. In this facility a control valve is installed to regulate the flow rate of the compressed air into the wind tunnel. The ability of the control valve to maintain a constant and steady pressure is essential because it dictates the stability of the exit jet velocity. To achieve a good performance the control algorithm should include a feedback loop. When a set point (pressure) is initiated from the input box, the control valve will respond to the command by opening the valve diaphragm first. Then the internal pressure reading at about 8-10 times diameter downstream of the control valve will be fed to the control algorithm of the control valve and compared with the set point pressure. The valve diaphragm will be adjusted automatically in a continuous and iterative manner to maintain a constant downstream pressure as close to the set point pressure as possible.

In the present design, the valve is installed with 8" pipes that contain highly pressurised gases with enormous amount of potential energy at the valve's inlet. Upon creating a considerable pressure loss at the valve's outlet, the potential energy

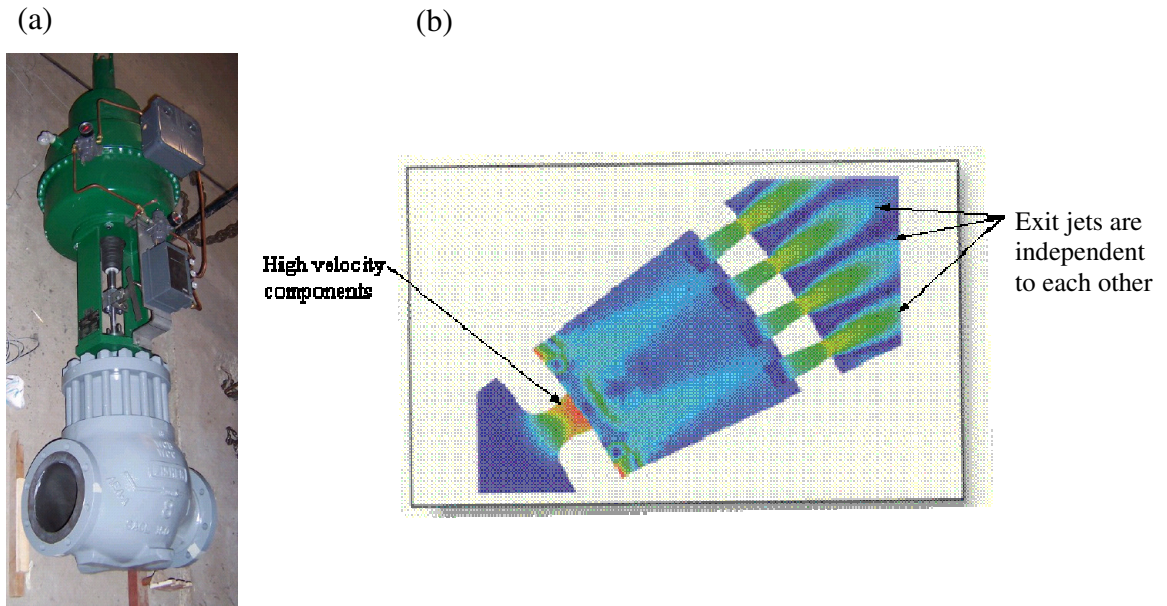


**Fig 3.** (a). Photo showing the WhisperFlo Trim Control Valve,  
 (b). CFD evaluation of flow through the control valve

is converted into other forms such as heat, vibration in piping and noise. Of all the energy forms, the valve noise represents the most severe noise generation mechanism in the wind tunnel. To this end, two approaches were employed to mitigate this shortcoming. The first is to search from the market to identify a control valve with innovative noise-control design; the second is to build a silencer downstream of the control valve to further attenuate the noise levels. The latter approach will be discussed in detail in the next section.

The control valve is finally chosen to be the WhisperFlo Trim, manufactured by Fisher® and shown in Fig. 3a. It is sized to withstand 2000kPa upstream pressure and reduce to a maximum downstream pressure of 200kPa across the valve. Several noise management techniques adopted by this control valve had enabled it to outperform other conventional types in terms of acoustical treatment. These are:

1. It divides pressure drop over two stages. It is designed such that the largest pressure loss occurs at the first stage, thereby restrict the largest acoustical conversion efficiency (hence the noise) locally. Since the pressure ratio of the second stage is minimised, the emitted noise is also reduced.
2. Special care is also taken to minimise shock-induced noise in the valve by a unique passage shape that is optimised to reduce flow turbulence. The shape can

also displace turbulent shear layer away from solid boundaries, which minimises aerodynamically dipole noise.

3. Jets may coalesce as they emerge from the cage, depends on the geometry of their exit paths. It is known that jet coalescence can cause additional noise source due to the enhanced turbulent mixing. The WhisperFlo Trim aligns the exit jets to be independent to each other. This specially treated exit path is assessed using CFD tool and the result is shown in Fig. 3b. From the figure, it is clear that jet coalescence doesn't occur. In addition, high velocity components (orange and red colour) are restricted in the first stage of the valve, leaving a relatively lower velocity at the second stage. This design enables most of the flow-generated noise to be contained within the cage.

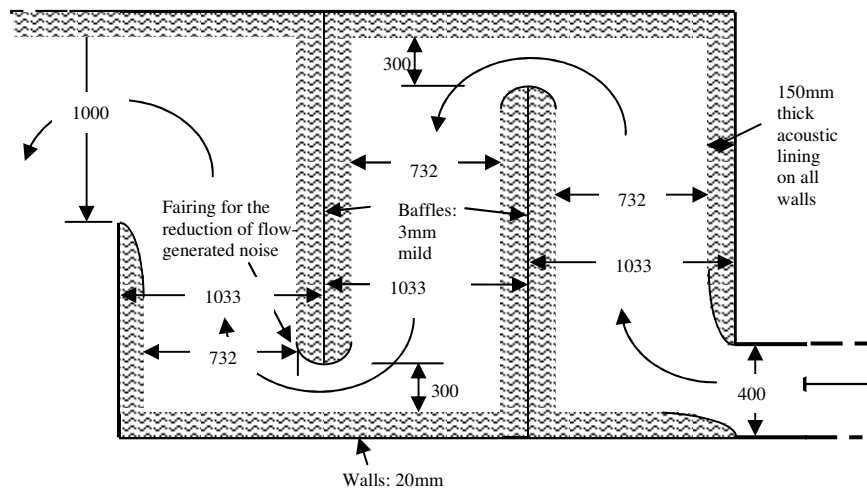


**Fig 4.** Schematic of the silencer. All units in mm

## 5.2. Primary Silencer

An additional silencer was designed and built to further attenuate the valve noise. The primary silencer is designed to have a high transmission loss (TL) and a low aerodynamic pressure drop. A schematic of the silencer is shown in Fig. 4. It is in the form of a lined “3 pass” plenum chamber, which incorporated two 90° acoustically lined bends and two 180° lined bends, in addition to three straight runs of lined duct. All interior surfaces are treated with the same dissipative liner, consisting of 150mm of Basalt wool, with a facing cloth (woven glass fabric) to inhibit flow delamination and a (mainly structural) facing of perforated metal. Figure 5 shows the details of acoustic lining in the silencer. Note that the thickness is evidently necessary in order to achieve the necessary sound transmission loss at

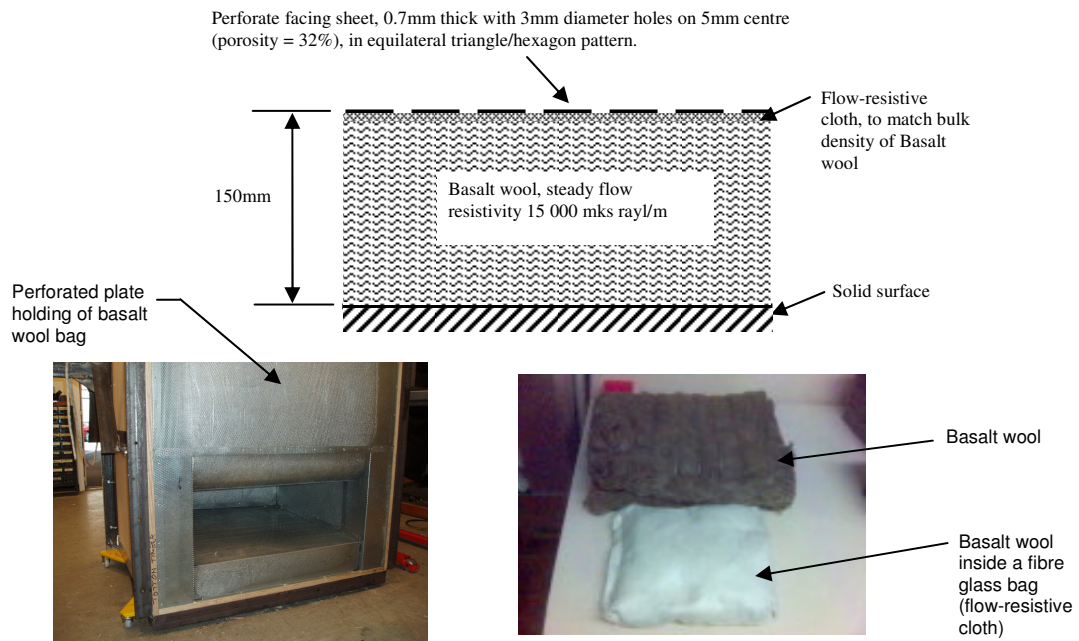


**Fig 5.** Details of acoustic lining in silencer

low frequencies. The frequency range of interest is assumed to be 200Hz-25kHz, the range over which the aerofoil generates appreciable acoustic power. The baffle plates are of mild steel, 3mm thick. This is in order to provide a sufficient transmission loss between successive “passes”, given that the lining will contribute significantly to the TL. The walls are made of 20mm plywood. Such thickness should be capable of reducing the direct structural flanking transmission (as opposed to “radiation bypass” flanking) within the silencer to acceptable levels. All these efforts should prove effective in reducing the radiation bypass or direct structural flanking transmission.

The acoustic linings at both of the 90° and 180° bends were originally featured flat tops with relatively sharp corner. In order to avoid the possibility of flow-separation noise, the geometry was modified in the final design where fairings are employed around the two 180° lined bend; while semi-hemispheres are trimmed at the two 90° lined bend.

An assessment of the primary silencer was performed. The arrangement of the experimental set up for quantifying the attenuator performance is shown in Fig. 6a. A loudspeaker was positioned near the entrance of the silencer and a white noise generator was used to drive the loudspeaker. The sound powers at the entrance of the silencer and the exit of the 4m rectangular straight passage in *Stage II* were then

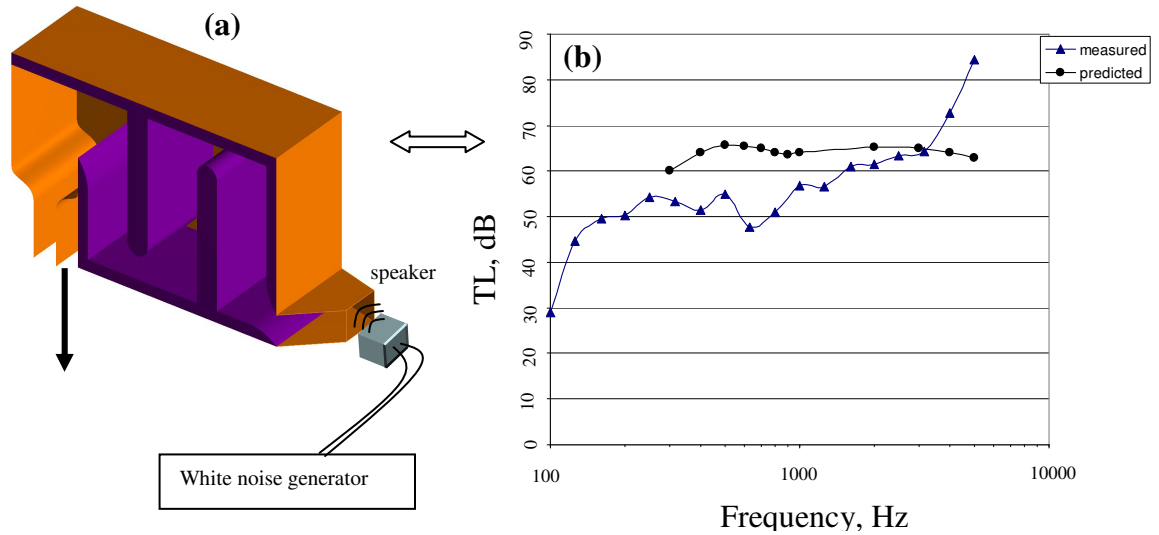


**Fig 6.** (a). Arrangement of the sound power test in no flow condition, (b). Comparison of transmission loss between experimental results and theoretical estimation

measured by traversing a B&K sound intensity probe of the respective areas. The ratio of sound powers at the inlet and outlet gives the sound transmission loss of the silencer. The result is compared with the theoretical model of Cummings<sup>13</sup>, for a frequency range of 200Hz-25kHz<sup>ii</sup>, as shown in Fig. 6b. Satisfactory agreement between the experimental result and prediction can be seen from the figure where 50 – 60 dB TL was obtained in the frequency range from 300 to 4000 Hz.

### 5.3.90<sup>0</sup>-Curved Diffuser

When the air leaves the 4m straight air passage and enters *Stage II*, it needs to be turned 90 degree anticlockwise towards the direction of the anechoic chamber. As mentioned earlier the inlet area of the nozzle should be between 1.35 – 1.70m<sup>2</sup>. With the exit area of the air passage fixed at 0.43m<sup>2</sup> (0.33 x 1.3m), an area expansion ratio of 3 – 4 is required. A 90<sup>0</sup>-curved diffuser is thus required to match these constraints.

A diffuser is generally used to recover static pressure and to expand the flow area. The 90<sup>0</sup>-curved diffuser in the current design serves the purpose of simultaneously

<sup>ii</sup> The predictive software for the silencer design was written on the basis of the low frequency wave model and the high frequency statistical model described by Cummings<sup>13</sup>, with modifications to take into account (i) a perforated facing sheet and a flow-resistive facing cloth over the absorbent, (ii) grazing mean flow effects on the lining impedance (though not on the sound propagation in the interior spaces of the silencer). Furthermore, a numerical scheme was incorporated to find accurate values of the various transverse wavenumbers employed in the low frequency model. Locally reacting behaviour was assumed for the acoustic lining.

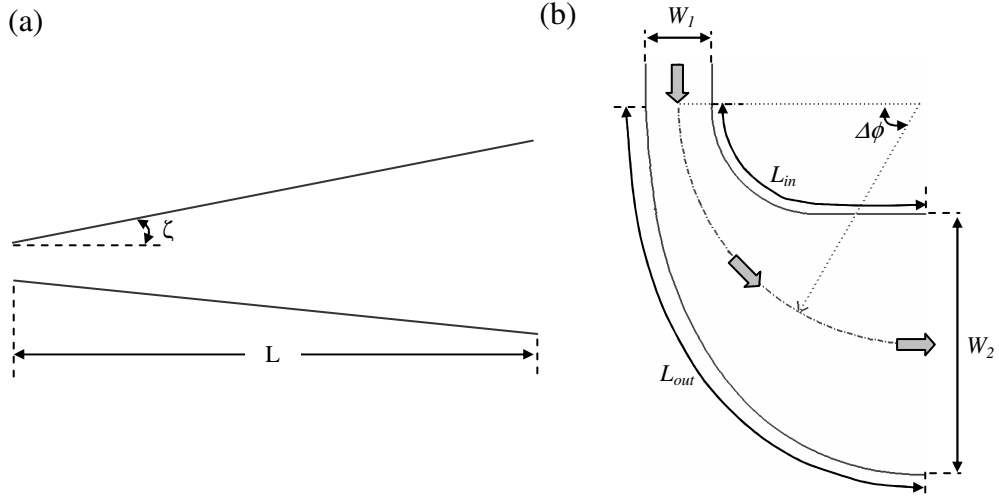


**Fig. 7** (a). A schematic depicting the parameters needed to describe (a). straight diffuser, (b). curved diffuser.

expanding the flow area and turning the flow path. It is of secondary importance for pressure recovery since the pressure at the curved-diffuser inlet has already been sufficiently large at about 80kPa. Unlike a straight diffuser, an effective curved-diffuser is more difficult to design due to the existence of centrifugal forces that can produce detrimental secondary flows. The combination of the pressure-driven secondary flow and the streamwise adverse pressure gradient makes the boundary layer more susceptible to flow separation, especially at the inner-wall region (convex part of the curved diffuser). When flow separation happens, not only the pressure fluctuations will result in noise emission, but also increase the turbulence intensity of the free jet. Ultimately, the acoustic and aerodynamic performances of a wind tunnel will be jeopardised.

Figures 7a and b illustrate the parameters needed to describe a two-dimensional straight diffuser and curved diffuser respectively. As a rule of thumb, it is more desirable to construct a straight diffuser with a small diverging angle,  $\zeta$  and long wall length,  $L$ , i.e. giving small  $\zeta/L$  ratio to avoid flow separation. For a curved diffuser, the larger the curvature,  $\Delta\phi$ , the more unstable the flow is likely to be. To be more precise, the growth of the boundary layer at the inner-wall is more crucial as opposed to the outer-wall (concave counterpart). Because of the curvature effect, the secondary flows in the mainstream inject low momentum fluids into the inner-wall shear flow<sup>14</sup>. As a result, the boundary layer will be thickened, causing it to possess less energy to sustain the region of increasing pressure. Moreover, the convex nature

of the inner-wall will also decrease mixing, thereby inhibiting the momentum exchange between inner and outer parts of the boundary layer. All these consequences cause the inner-wall boundary layer to be more susceptible to flow separation.

Figure 8 shows the design conditions with regard to stall (analogous to flow separation) for curved diffuser with a quadrant inner-wall from  $\Delta\phi = 0^\circ - 90^\circ$ . The data points in the figure were compiled by Sagi and Johnston<sup>15</sup>. The abscissa is the scaled inner-wall length,  $L_{in}/W_1$  and the ordinate is the area ratio ( $AR$ ),  $W_2/W_1$ . Here  $W_1$  and  $W_2$  are the

widths of the curved-diffuser inlet and outlet respectively and  $L_{in}$  is the inner-wall length. Each line in Fig. 8 represents the first stall limit for its respective turning angle,  $\Delta\phi$ . Curve diffusers should be constructed such that the above dimensionless parameters fall below the stall line to achieve stable flow. From the figure, It has been demonstrated that, to maintain separation-free at the inner-wall region, the allowance for higher  $AR$  and lower  $L_{in}/W_1$  decreases when  $\Delta\phi$  increases. In other words, to maintain a steady diffusing flow more floor space is needed.

However, for the current design, there is a severe space limitation to expand and turn the flow  $90^\circ$  anticlockwise towards the anechoic chamber (with only 2.4m in height between the ceiling and the floor). A short curved-diffuser is therefore inevitable which results an inner-wall with abrupt curvature. With the available space and the required curved-diffuser expansion ratio of 3 – 4 as the only two constraints, the  $90^\circ$ -curved diffuser for the current wind tunnel was designed accordingly.  $W_1$ ,  $W_2$  and  $L_{in}$  were finalised as 330, 1300 and 849mm respectively. This configuration yields  $L_{in}/W_1$  as 2.57 and  $W_2/W_1$  (or  $AR$ ) as 3.94 with  $\Delta\phi = 90^\circ$ . If these values are substituted into Fig. 8, it is apparent that the current  $90^\circ$ -curved diffuser which bears some rather short  $L_{in}/W_1$ , large  $AR$  and large  $\Delta\phi$  characteristics will fall into a severe stall regime for a wide range of Reynolds numbers.

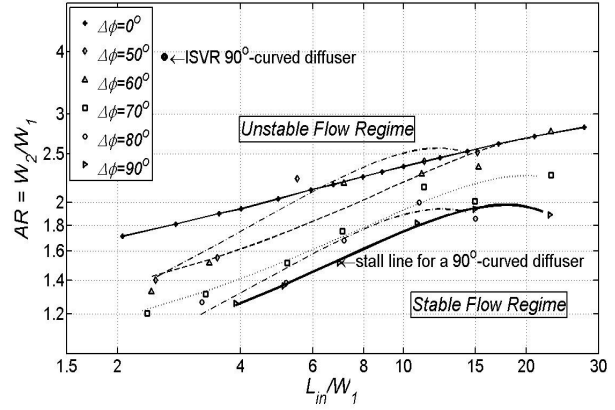


**Fig 8.** Location of first appreciable stall as a function of  $\Delta\phi$  for curved diffuser with quadrant inner-wall shape<sup>14</sup>.

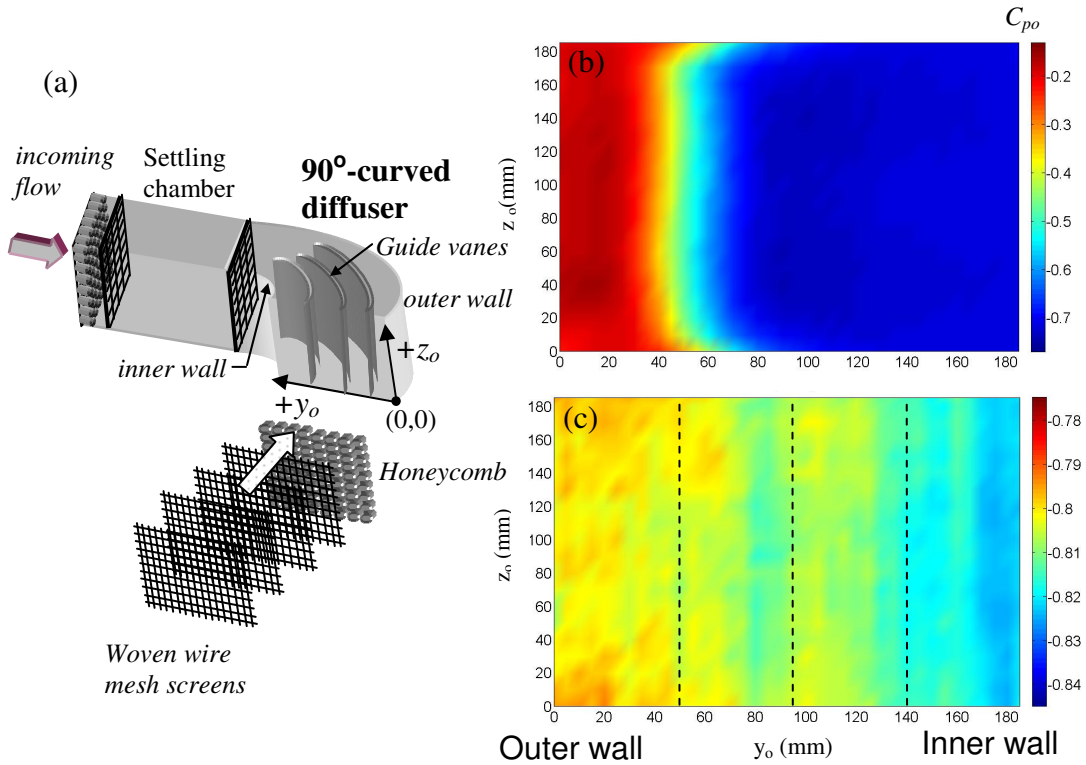


**Fig. 9** (a). Schematic of the 90°-curved diffuser model for the flow control study. Coordinate system for the diffuser exit flow is also shown. Contours of exit pressure coefficient,  $C_{po}$  for the 90°-curved diffuser (a). without flow control, (b). with three guide vanes (location indicated by the vertical dash lines) and  $5.5q$  pressure drop at the exit. Negative values of  $C_{po}$  is caused by the discontinuity of total head between the reference and the measurement points as the result of flow through screens.

To achieve a non-separating boundary layer with this geometry the diffusing flow should be controlled at the expense of a smaller pressure recovery at the exit. Several passive flow control methods have been proposed, which include splitter vanes, honeycomb and woven wire mesh screens. Prior the construction of the 90°-curved diffuser, a  $1/6^{\text{th}}$  scaled-down model was first fabricated and attached to a centrifugal blower to parametrically study the optimum combination of the aforementioned flow control devices. A schematic that depicts these is shown in Fig. 9a. A pitot tube was used to measure the cross-sectional total pressure contours at 5cm from the diffuser model exit. These pressure contours, which reveal the degree of flow uniformity improvement after applying flow controls, are shown in Figs. 9b and 9c. Figure 9b shows the pressure contours in the absence of splitters, honeycomb and screens. It is apparent that a significant total pressure deficit (blue colour) encompasses more than 50% of the flow area at the exit. This pressure deficit region is associated with the large-scale, non-recoverable flow separation that originated from the inner-wall region. A consequence of the “dead flow” regions

shown in Fig. 9b is that most of the mass flow is transferred to a fast stream flow towards the outer-wall region. Without flow control treatment, incorporating the current 90°-curved diffuser into a wind tunnel would require a substantial distance before the separated flow from the diffuser inner-wall reattaches again. Following extensive testing, it is claimed that three equally spaced splitter vanes, a honeycomb at the diffuser exit followed by three fine woven wire mesh screens, with a cumulative pressure drop of  $5.5q$  ( $q$  is the dynamic pressure, see Eq. 2) can suppress effectively

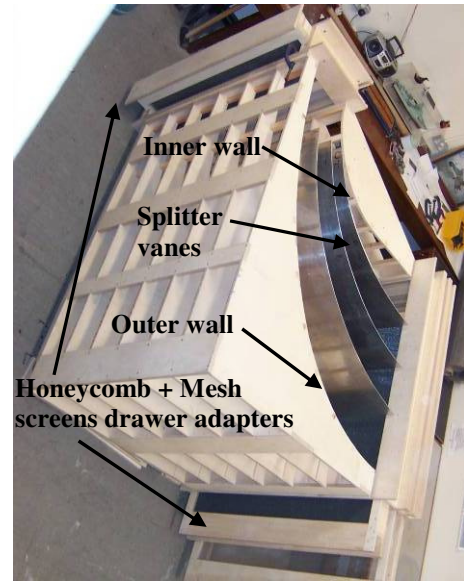


**Fig. 10** Inner structure of the 90° curved full-size diffuser with guide vanes, honeycomb and screens.

boundary layer separation at the inner-wall<sup>iii</sup>. This can be confirmed in Fig. 9c where the exit flow was found to be reasonably uniform over most of the exit area (note that the contour scale in Fig. 9c is narrowed to increase the resolution, i.e. if the same larger contour-scale as in Fig. 9b is used instead, a visually more uniform pressure distribution will be obtained). Detailed discussion of the physical mechanism of the screens to inhibit flow separation is out of scope here but will be reported elsewhere<sup>16</sup>.

This combination of splitter vanes, honeycomb and screens was finally adopted in the full size 90°-curved diffuser, as shown in Fig. 10. Composite drawer adapters for honeycomb and mesh screens were also installed at the inlet and exit of the diffuser. This drawer adapter features a rail type handling system that allows a simple changeover of mesh screens. After the diffuser was constructed and connected to the vertical air duct inside an anechoic chamber, a rake of 9 pitot tubes covering the distance between the outer to inner-walls of the diffuser (~1.3m) was used to simultaneously measure the exit flow total pressures. Since the full-size and scale-model experiments were performed at different flow speeds, collapse of data between the two is not possible. A more meaningful approach would be to

<sup>iii</sup> It is also observed that the exit flow uniformity can be further improved by adding more guide-vanes and larger pressure drop at the curved-diffuser exit. The suggested combination is a good balance of effective flow control and minimal construction complexity.

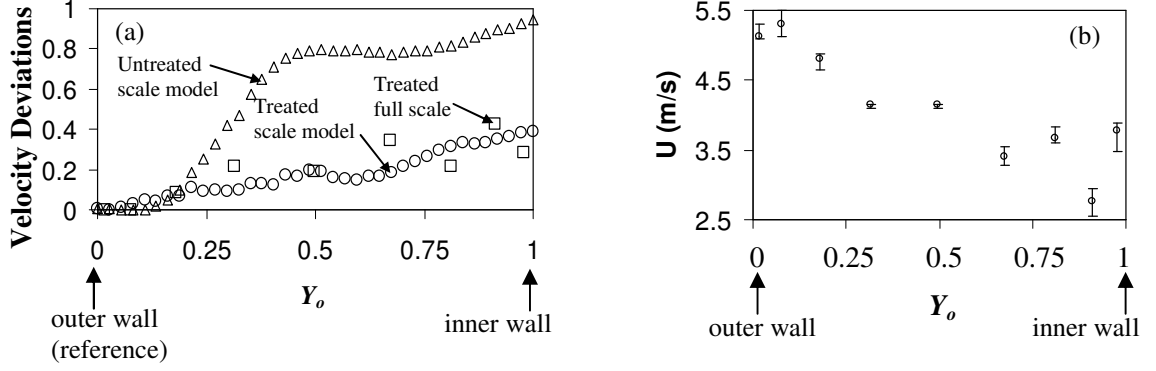


**Fig. 11** (a) Comparison of velocity deviations from outer to inner walls at  $Z=0.5$  of the  $90^\circ$ -curved diffuser exit for:  $\circ$  – treated scale-model,  $\Delta$  – bare, untreated scale-model and  $\square$  – treated full size  $90^\circ$ -curved diffusers; (b). Distributions of exit velocity at different spanwise locations,  $z$  from the outer to inner walls of the full-size  $90^\circ$ -curved diffuser.

determine the velocity deviations,  $U_{dev}$ , of the measured velocity compared with the flow at the outer wall region where it is usually of maximum. This quantity can be expressed as:

$$U_{dev} = \frac{U_{(Y_o \rightarrow 0, Z_o=0.5)} - U_{(Y_o, Z_o=0.5)}}{U_{(Y_o \rightarrow 0, Z_o=0.5)}} \quad (1)$$

where  $U_{(Y_o \rightarrow 0, Z_o=0.5)}$  is the velocity at the outer wall region of the centre-plane,  $Z_o=0.5$ ; whereas  $U_{(Y_o, Z_o=0.5)}$  is the velocity from the outer to inner walls (in  $Y_o$  direction), also at  $Z_o=0.5$ . Here  $Y_o$  and  $Z_o$  are the normalized distance of  $y_o$  and  $z_o$  respectively, and both have values from 0 to 1. Figure 11a compares the aerodynamically treated full-size ( $\square$ ) and scale-model ( $\circ$ ) velocity deviations at  $Z_o=0.5$  of the  $90^\circ$ -curved diffuser exits. Also shown in the figure is the corresponding velocity deviation for a bare, untreated scale-model  $90^\circ$ -curved diffuser ( $\Delta$ ). Good agreement is observed between the flow uniformities of the full-size and scale-model diffusers with flow treatment. For the treated case, the velocity deviations of exit flow from the outer to the inner walls for both of the full-size and scale-model diffusers are significantly lower than the untreated case. This implies that the addition of splitter vanes, honeycomb and pressure-reducing screens has successfully maintained uniform flow over a relatively wide range of Reynolds numbers by inhibiting large-scale flow separation at the inner wall. Finally, error bars that correspond to the distributions of exit velocity at different spanwise locations ( $Z_o$ ) from the outer to inner walls are shown in Fig. 11b. The deviations are generally small which implies that a satisfactory two-dimensional exit flow has

been achieved by the uses of both guide vanes and mesh screens. With the 90°-curved diffuser running at the maximum mass flow rate of 8kg/s, acoustical assessment of the facility noise inside the anechoic chamber was performed. It was done by measuring the sound pressure level at 3m from the diffuser exit at a polar angle of 0

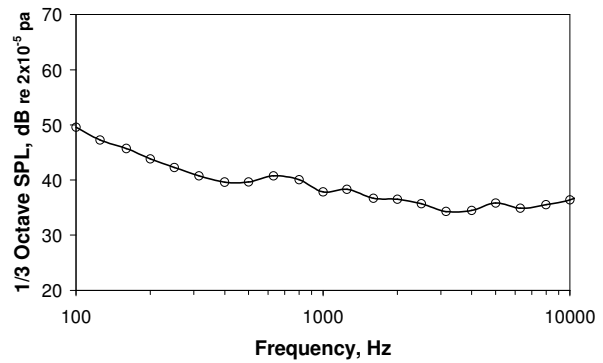


**Fig. 12** 1/3 octave sound pressure level of the 90°-curved diffuser exit flow at mass flow rate of 8kg/s. Measurement was taken at 3m from the centre of the diffuser exit at polar angle of 0 degree.

degree. The instrument for the noise measurement was a B&K ¼-in. type 2670 condenser microphone covered with windshield. Although no comparison is made against any form of prediction, the experimental result in Fig. 12 shows a reasonably broadband spectrum with low noise level for a wide frequency range. This spectrum was later referred to when designing the ensuing settling chamber. Description of this process is presented in the next section.

#### 5.4. Settling Chamber / Secondary Silencer

It is beneficial, from an aerodynamic point of view, to install a straight duct following the 90°-curved diffuser to smoothen the flow before it enters the nozzle. This component is often called “settling chamber” and one with an overall dimension of 1.3 x 1.3 x 2m was added to the current open jet wind tunnel. Supplementary flow management devices such as honeycomb and screens were also included at both of the inlet and outlet of the settling chamber. Note that the honeycomb and screens at the settling chamber inlet are indeed the very same devices for the boundary layer separation control of the 90°-curved diffuser. Considering the associated high local pressure drop from the screens, it is therefore sensible to choose the region where low velocity is located (at the 90°-curved diffuser exit) so that their role in the overall pressure drop in the open jet wind tunnel is minimised.

Honeycomb is primarily used to straighten the flow and to reduce lateral velocity fluctuations. It also can, to a certain extent, breaks up eddies that are larger in size than the cell dimension. In choosing the honeycomb, a minimum 8 – 10 cell diameter is required for the length<sup>18</sup>. This is to ensure that sufficiently long passage

is provided for the skewed flow in each cell to regain straightness. In this case, two honeycombs with 63.5mm long and hexagonally shaped with cell diameter of 6.35mm were installed at both of the settling chamber's inlet and exit. The honeycombs are made of commercial grade aluminium (Type 3003) with density of 83Kg/m<sup>3</sup>.

However, honeycomb is less capable of reducing the streamwise component of the flow fluctuation and non-uniformity (eddies smaller than the cell size). In addition, it also can produce some eddies of its own, with the sizes of the same order as the cell diameter. This could increase the turbulence level in the freestream. In modern wind tunnel design, screens were commonly inserted behind the honeycomb to further improve the flow quality. An important criterion for choosing the right screen lies in its pressure drop characteristics. In incompressible flow, the pressure drop coefficient of a screen,  $K$  can be expressed as<sup>17</sup>:

$$K = \frac{\Delta p}{q} = A \left( \frac{1}{\beta^2} - 1 \right)^B \quad (2)$$

where  $\Delta p$  is the pressure drop across the screens,  $q$  is the upstream dynamic pressure and  $\beta$  is the porosity, where  $A$  and  $B$  are constants that are usually taken as 0.52 and 1 respectively for square woven type of mesh screen. Figure 13 shows a simple drawing of a screen needed to describe the porosity,  $\beta$ . From Eq. (2), the pressure drop characteristic of a screen can solely be determined by its porosity.

Based on experience from the parametric study of the scaled-down 90°-curved diffuser experiment, it was concluded that a large cumulative  $\Delta P$  is recommended to achieve uniform flow. On the other hand, the use of single screen with porosity,  $\beta$  less than 0.5 ( $\Delta P > 1.56q$ ) is not recommended, with  $\Delta P \approx 2.0q$  being the upper limit<sup>18</sup>. This is to avoid instability caused by jet coalescence. Moreover, too small of wire diameter should be avoided (although this has advantage of turbulence reduction). This is because that in doing so, a small pitch is required in order to keep

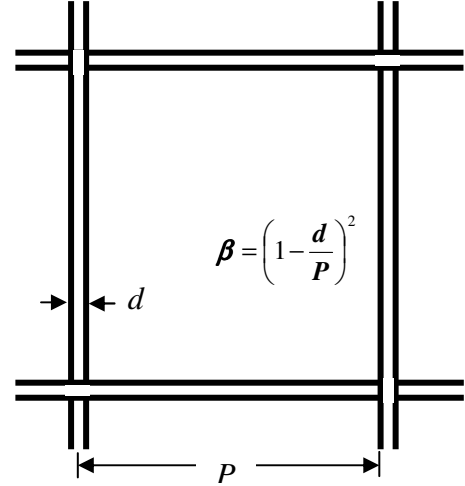


**Fig 13.** Definition of mesh width and porosity

Honeycomb	Cell Diameter (mm)	Cell Length (mm)		
H <sub>1</sub>	6.35	63.5		
H <sub>2</sub>	6.35	63.5		
Screen	D (mm)	P (mm)	$\beta$	K
S <sub>1</sub>	0.33	1.01	0.45	2.0
S <sub>2</sub>	0.33	1.01	0.45	2.0
S <sub>3</sub>	0.36	1.36	0.54	1.5
S <sub>4</sub>	0.4	1.7	0.58	1.0
S <sub>5</sub>	0.3	1.28	0.58	1.0

**Table 2** Data for the honeycombs and screens used in the open jet wind tunnel. Refer to Fig. 2 for locations of the various honeycombs and screens

the porosity constant. Consequently, particles and dusts in the flow can easily be trapped and subsequently generate extraneous vortex shedding to increase the fluctuation level in the main flow. In this manner the use of screens to dissipate flow turbulence is no longer effective. As a compromise, it is more desirable to employ several small-“K” screens to accumulate an overall larger pressure drop. Summary of the screens used in this wind tunnel is presented in Table 2.

The settling chamber can also be acoustically lined to further attenuate the residual valve noise and the possible flow-induced noise. The settling chamber in this way is said to be upgraded to a secondary silencer. After all, the 90°-curved diffuser indeed features a critically unfavourable geometry that is prone to generate pressure fluctuations in the flow and radiate noise. The addition of splitter vanes inside the diffuser could produce extraneous noise as a result of flow impingement and growth of boundary layers. Note that it is difficult to trace from Fig. 12 the individual level of contributions from the different noise sources listed above. A more general approach to design the acoustic liners inside the settling chamber is to

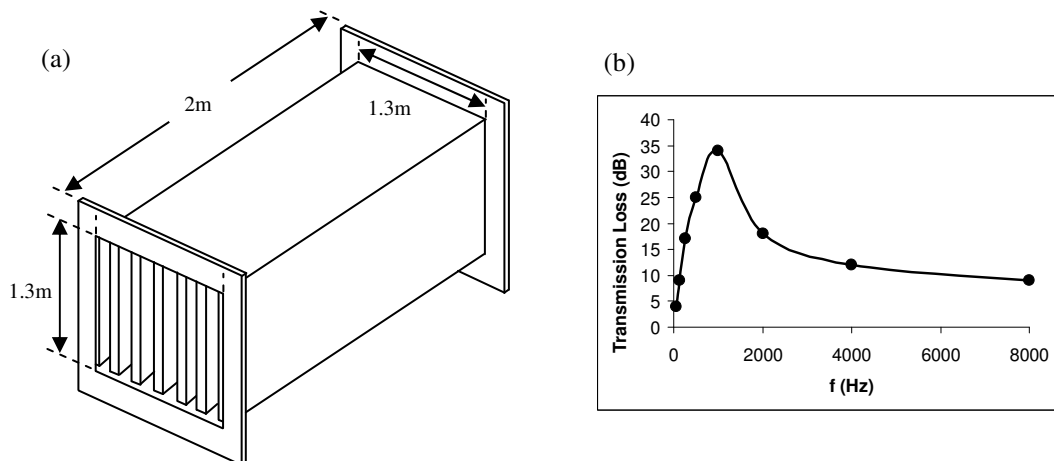


**Fig. 14.** (a) Isometric view of the settling chamber with lined splitters; (b) Predicted transmission loss of the acoustically-lined settling chamber.

take the spectrum of Fig. 8 as the reference noise level and compare it with the predicted airfoil trailing edge noise spectrum. The addition of an optimised secondary silencer is seen as an essential approach in achieving the principle target of “aerofoil trailing edge noise must be at least 10dB above the facility noise” in this work.

The method of Kurze<sup>19</sup> was used to predict the transmission loss for different combinations of lined-splitter numbers and their thickness. In the final design, the acoustic liner consists of five parallel absorptive lined-splitters and two lined-sideliners, as shown in Fig. 14a. The lined-splitters are 1800mm in length and 110mm in thickness; whereas the sideliners are 40mm in thickness. Acoustically transparent perforated metal sheets were used to cover both. They also feature super-elliptical leading edge and tapered trailing edge shapes to ensure that smooth and attached flows exist on the splitter walls. The overall pressure drop caused by the growths of the boundary layer displacement thicknesses on the splitter walls was estimated to be around a negligible level of 90Pa. The predicted transmission loss for this configuration is shown in Fig. 14b. From the figure it is clear that large noise reduction occurs from 250 – 2000Hz, the frequency range over which substantial acoustic power is generated at the aerofoil trailing edge.

## Nozzle

The flow is accelerated rapidly in the nozzle resulting in large streamwise strain. The choice of large contraction ratio such as the present one (25:1 area ratio), which is directly proportional to the strain in the streamwise direction, is useful for minimising flow non-uniformity and streamwise velocity fluctuations. However, the use of a large contraction ratio nozzle also carries the risk of causing flow separation near the ends. In general the radius of curvature at the ends can be small to avoid separation but this will result in longer contraction length and an increase of exit boundary layer thickness. In addition, the nozzle consists of concave (at upstream) and convex (at downstream) parts so the inflection point should be designed such that the first and second derivatives of the nozzle profiles are as small as possible.

The present nozzle is designed as a three-dimensional, 25:1 area ratio nozzle. The inlet of the nozzle is a square section measuring 1.3 x 1.3m and the outlet is rectangular shape measuring 0.15 x 0.45m. The axial length of the nozzle is 1.35m.

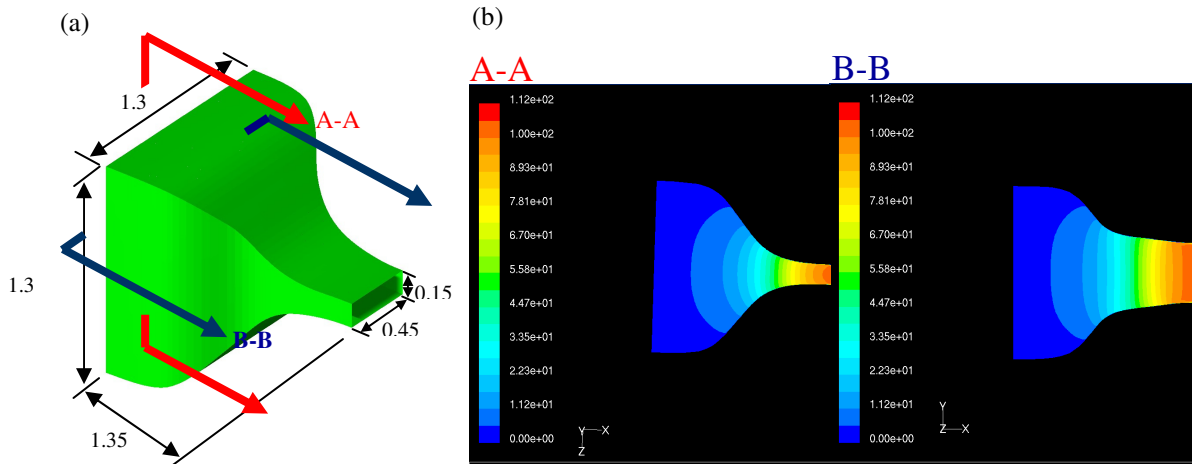


**Fig. 15** (a). Isometric view of the 3D nozzle, all units in m, (b). Numerical results of the flow field inside the nozzle, presenting velocity contours at A-A and B-B planes.

An isometric view of the nozzle is presented in Fig. 15a. The design is then evaluated numerically by performing steady, RANS calculation using  $k-\epsilon$  turbulence model. As shown in Fig. 15b for the velocity contours, no flow separation is predicted inside the nozzle.

Special care was taken to manufacture the nozzle. For structural rigidity the material for the nozzle was chosen as 3mm zinc-plated mild steel. The steel plates were first cut and formed into shape by an in-house sheet metal folding machinery. Once formed, they were welded together to form the shape as depicted in Fig. 15a. For this facility no flanges were used as the connecting pieces. This is to avoid possible distortion of the nozzle when the flanges are welded to the skins. Instead, a large wooden frame was attached to the nozzle inlet to be used as a connecting piece. A steel structure with castors was manufactured to support the nozzle and the wooden framework.

## 6. Calibration of the Open Jet Wind Tunnel

Figures 16a and b show the completed control valve and primary silencer in *Stage I* (see Fig. 2) as well as the  $90^\circ$ -curved diffuser, acoustically-lined settling chamber and nozzle in *Stage II* (see Fig. 2) inside the ISVR's anechoic chamber respectively. Since each wind tunnel components such as the primary silencer,  $90^\circ$ -curved diffuser and acoustically-lined settling chamber had already been calibrated and characterised separately (*Phase II* of Fig. 1), this section describes the global facility background noise as the function of different exit jet velocity (*Phase III* of

**Fig. 16** Photos of the completed components of (a). *Phase I*, (b). *Phase II* (inside the ISVR anechoic chamber). Note that the coordinate system in reference to the nozzle is shown in (c).

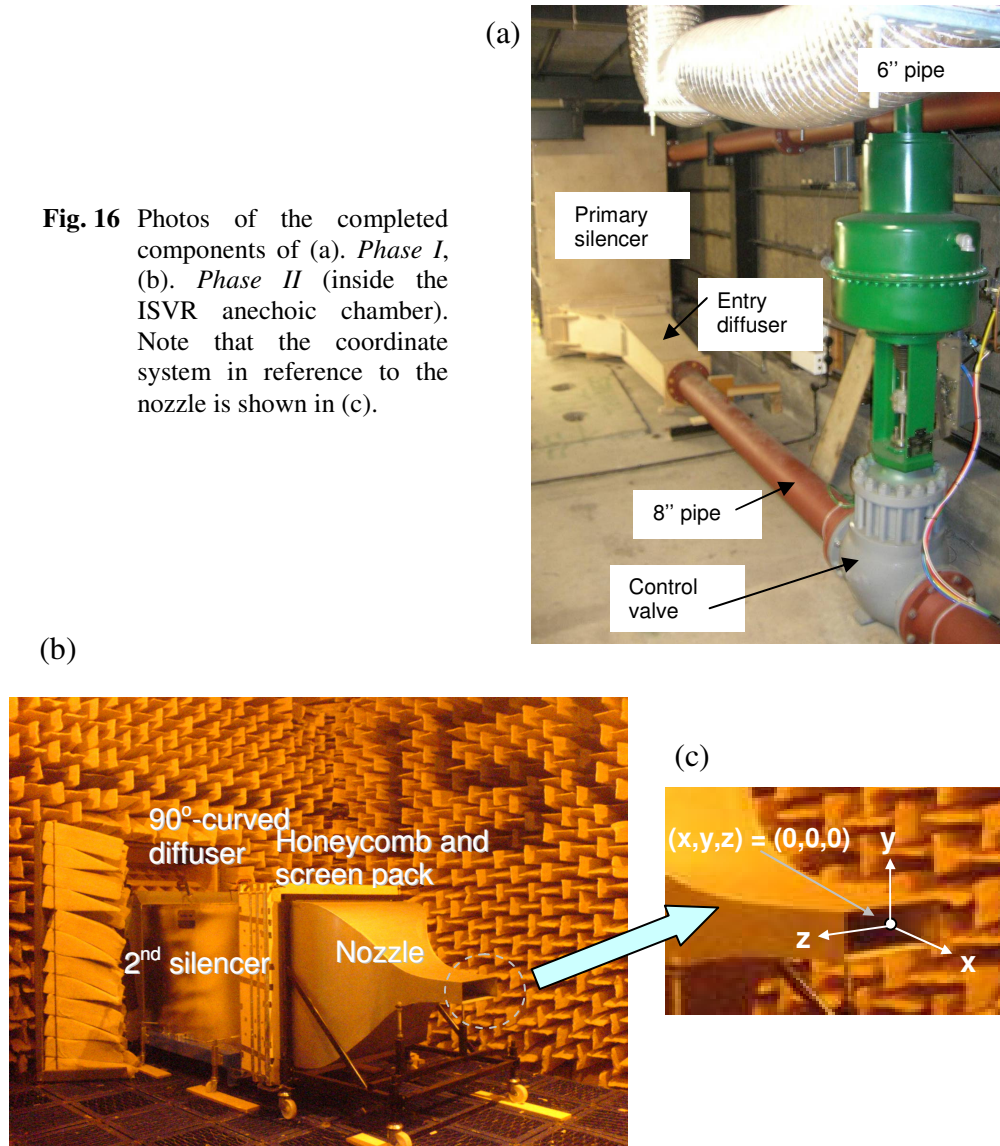
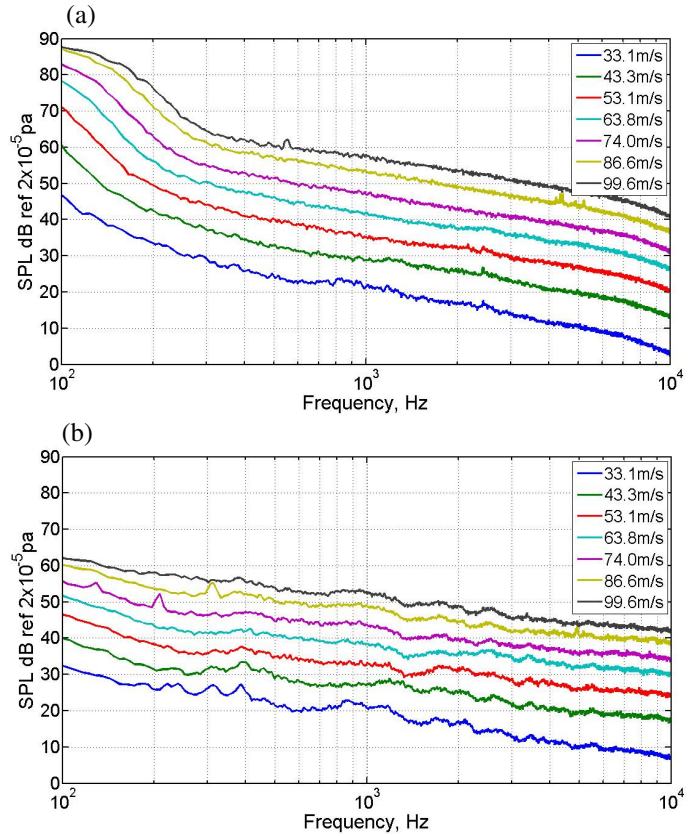


Fig. 1.). In addition, the flow uniformity and turbulence intensity of the exit jet were also measured and presented. Note that in the subsequent discussion both of the acoustic and aerodynamic calibrations always take the position reference to the nozzle exit, where the coordinate system is depicted in Fig. 16c.

### 6.1 Analysis of Background Noise Levels

A B&K ¼-in. type 2670 microphone was placed at  $(x,y,z) = (0, 0.5, 0)$ , i.e. 0.5m vertically above the centre of the cross-sectional nozzle exit plane to measure the background noise level inside the anechoic chamber at different exit jet velocity. This corresponds to  $90^\circ$  polar angle,  $\theta$ . Here  $\theta$  is defined as the angle from the jet axis. In addition, an electret microphone (Behringer ECM8000) was placed at  $\theta =$

$45^\circ$  (0.45, 0.35, 0) to account for the directivity of the exit jet. Figures 17a and b show the narrowband sound pressure level at  $\theta = 45^\circ$  and  $90^\circ$  respectively pertaining to the open jet wind tunnel when operated at jet velocities from 33.1 to 99.6ms<sup>-1</sup>. These figures are plotted in the form of power spectra density with a 1 Hz bandwidth and a frequency resolution,  $\Delta f$  of 6.25Hz. From the figure, the spectra feature a reasonably linear decay of sound pressure level in log frequency scale. However, it is difficult to discern from Fig. 17a and b which noise source is dominant at a particular frequency range.



**Fig. 17** Sound pressure level, dB (ref  $2 \times 10^{-5}$  pa) at 1Hz bandwidth,  $\Delta f = 6.25$ Hz of the open jet wind tunnel operated from jet velocities 33.1 – 99.6m/s. Spectra measured at (a).  $\theta = 45^\circ$ , (b).  $\theta = 90^\circ$

Another approach is to analyse how the sound pressure level varies with jet velocity as the function of frequency. Figure 18 shows the dependency of sound pressure level on jet velocity,  $\overline{p^2} \propto V^N$  for  $\theta = 45^\circ$  and  $90^\circ$ , where  $N$  is the power factor of the velocity. The analysis shows that for  $\theta = 45^\circ$ , the sound pressure level scaled with  $V^{7.5} - V^8$  between 400 – 10kHz. This is associated with quadruple aerodynamic noise such as the jet noise or free shear layer noise. For  $\theta = 90^\circ$ , the dependency of sound pressure level on velocity averages at  $V^{6.5}$  between 100 – 2kHz. This velocity dependency implies that dipole aerodynamic noise is dominant at this measurement angle. The possible noise sources are those produced by the nozzle lip noise, which should bear close resemblance to the edge self-noise. Another possible dipole noise contributor at this frequency range could be due to the noise breakout from inside of the rig. From 2kHz onwards, the sound pressure level fits the  $V^7$  scaling law, indicating the influence of jet noise.

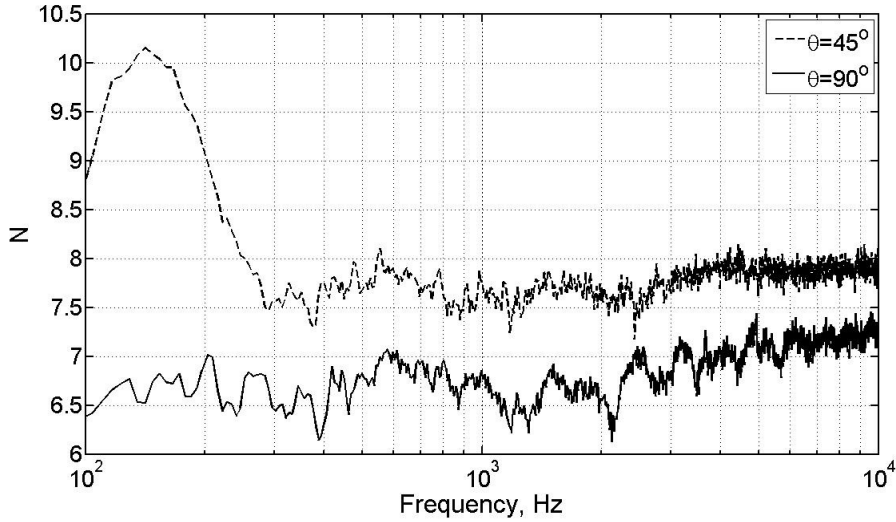


**Fig. 18** Dependency of sound pressure level on jet velocity for ---  $\theta = 45^\circ$  and -  $\theta = 90^\circ$ . Note that  $N$  is the power factor of the velocity.

After the dependency of sound pressure level on jet velocity as the function of frequency is established, the analysis continues on the variations of overall sound pressure level (OASPL) on jet velocity. OASPL is obtained by integrating the mean square pressure over a frequency range. Figure 19 shows the correlations of OASPL with jet velocity for  $\theta = 45^\circ$  and  $90^\circ$  respectively. Nota that the A-weighted OASPL are also included for comparison. From the figure, the OASPL is scaled with  $V^{4.6}$  and  $V^{5.3}$ , whereas the A-weighted OASPL exhibits  $V^{7.6}$  and  $V^{6.8}$  dependency on jet velocity for  $\theta = 45^\circ$  and  $90^\circ$  respectively. In comparison with the velocity scaling

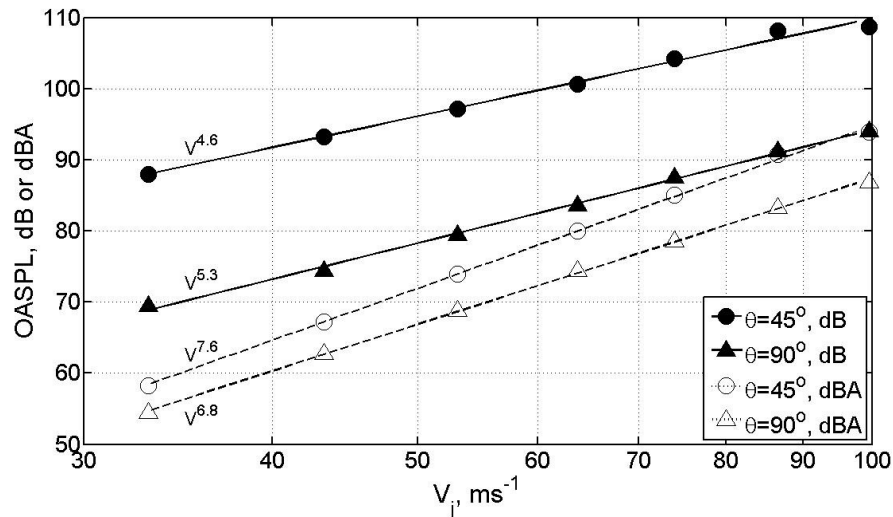


**Fig. 19** Distributions of OASPL with jet velocity for  $\theta = 45^\circ$  and  $90^\circ$ . Power factors of the velocity  $N$  are indicated for both of the dB and dBA cases.

factors between the normal and the A-weighted OASPL, the latter correlates better with results in Fig. 18 for frequency range of 300 – 10kHz. This is due to the attenuation effects of A-weighting on low- and high-frequency mean square pressures.

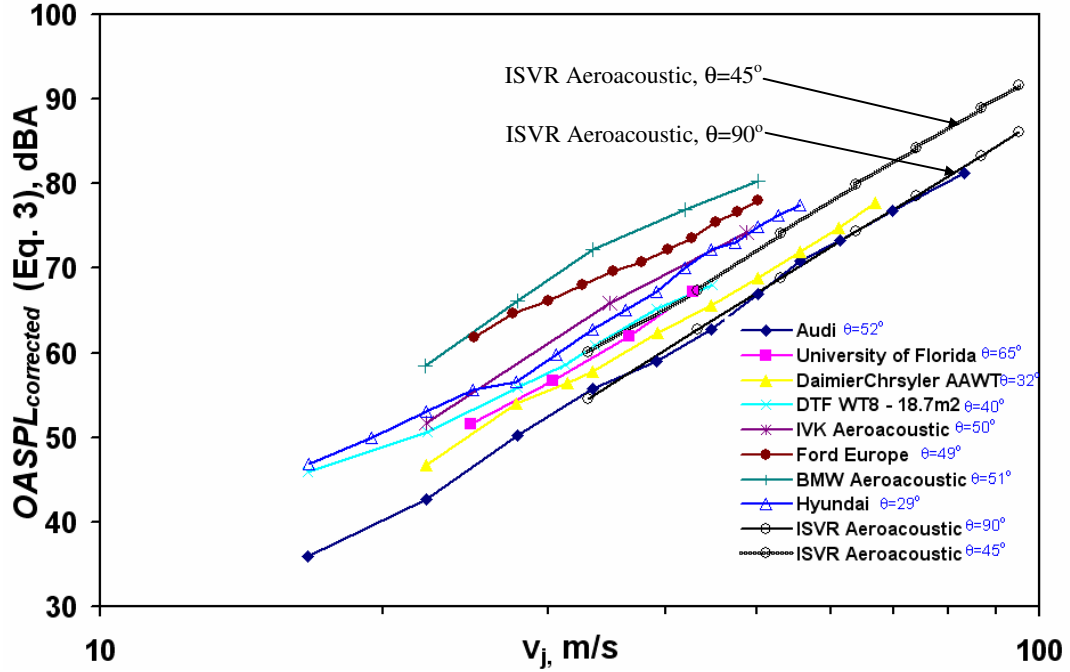


**Fig. 20** Comparison of A-weighted OASPL (corrected by Eq. 3) background noise of the current open jet wind tunnel to the other worldwide facilities.

An attempt is made to compare the results in Fig. 19 with other automobile and aeroacoustic wind tunnels in previously published data<sup>9-11</sup>, where distributions of OASPL with test section velocity are available. Note that the OASPL herein refers to the noise measured outside of the flow, and the microphone locations relative to the plane of their nozzle exits are different. With the assumption of negligible variance of sound radiation in the azimuth plane<sup>iv</sup>, the OASPL pertinent to the facilities in ref. [9-11],  $OASPL_{iFacility}$ , were corrected for distance  $r_{iFacility}$  and nozzle area  $A_{iFacility}$  to match the present open jet wind tunnel by the following equation:

$$OASPL_{corrected} \propto OASPL_{iFacility} + 10 \log_{10} \left( \frac{r_{iFacility}}{r_{ISVR}} \right)^2 - 10 \log_{10} \left( \frac{A_{iFacility}}{A_{ISVR}} \right) \quad (3)$$

<sup>iv</sup> For example, the OASPL at (0, 0.5, 0), (0, 0, 0.5), (0, -0.5, 0) and (0, 0, -0.5) are the same.

where  $r_{iFacility}$  is the distance from the microphone to the centre of the nozzle exit plane for each wind tunnels.  $A_{ISVR}$  and  $r_{ISVR}$  are  $0.0675\text{m}^2$  and  $0.5\text{m}$  respectively. Nota that Eq. 3 is also applicable to A-weighted OASPL. Figure 20 presents the distributions of A-weighted OASPL with test section velocity for a number of well-known automobile and aeroacoustic research wind tunnels around the world. Here the interception of the  $r_i$  line and the jet axis represents the polar angle  $\theta$ , and it is important to recognise that  $\theta$  is different for different wind tunnels presented in Fig. 20. The sound field from a jet is very directive, with the maximum noise being radiated in the annular region of  $30^\circ$  to  $45^\circ$  from the jet axis in subsonic flow<sup>20</sup>. Hence the data in Fig. 20 cannot be compared directly. The distributions of A-weighted OASPL with jet velocity at  $\theta = 45^\circ$  and  $90^\circ$  for the present case are included in the figure, with the result for  $\theta = 45^\circ$  representing the upper-limit case since the noise level is maximum at around this angle. Analysis of Fig. 20 reveals that the A-weighted OASPL at both  $\theta = 45^\circ$  and  $90^\circ$  for the present open jet wind tunnel is as good as, if not superior than most of the wind tunnels in terms of achieving low background noise. It is also shown that the increase of A-weighted OASPL scales with  $\log(V)^{7-8}$  for almost all of the wind tunnels presented, including the present ones. In general, the acoustic performance of the ISVR open jet wind tunnel is excellent and competitive, and the low-noise characteristic reflects the overall successful design that potentially capable of providing high signal-to-noise ratio for the aerofoil trailing edge noise measurements.

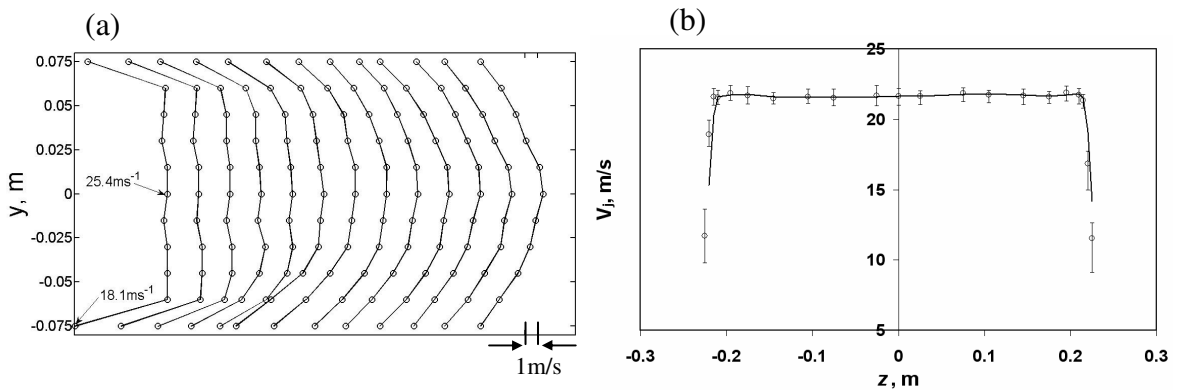


**Fig. 21** (a). Stakes of velocity profiles in the  $x$ - $y$  plane at  $z = 0$ . The velocity profiles starts at the left hand side of the figure from  $x = 0.1\text{m}$  and to the right hand side of the figure at  $x = 1.3\text{m}$  with  $0.1\text{m}$  increment, (b). Distribution of the velocity profiles averaging across the  $y$  axis at different spanwise location of the nozzle exit plane at  $x = 0.05\text{m}$ . Error bars corresponding to the upper and lower velocity limits at each spanwise location are also shown.

## 6.2 Analysis of Exit Flow Uniformity and Turbulence Characteristics

The aerodynamic performance of the open jet wind tunnel is as important as her acoustic counterpart. However, detailed exit flow mapping is more difficult to achieve in this wind tunnel due to the limited air discharging time for each run. To investigate the uniformity of the flow more efficiently, total pressure profile of the exit jet were simultaneously measured using a custom-made pitot-tube rake. The rake consists of eleven 1.2mm-internal diameter steel tubes with spacing of 15cm between each tube, which covers the whole height of the nozzle exit. With the static pressure equal to the atmospheric pressure for the open jet, the jet velocity can be deduced from the measured total pressure. The pitot-tube rake was attached to a computer-controlled two-dimensional traverse mechanism. The accuracy of the traverse is within  $\pm 0.1$ mm in both directions. Figure 21a shows the velocity profiles of the plane parallel to the jet axis (x-y plane) at  $z = 0$  between streamwise distance,  $x$  of 0.1 and 1.3m with an increment of every 0.1m. Although the spacing between each measuring point of the velocity profile (in y-axis) is relatively coarse, the figure still illustrates the transformation of the velocity profiles from an initially top-hat to a fully-developed shape downstream. This characteristic indicates the spreading of the momentum-deficit shear layers that were shed from the top and bottom nozzle edges by entrainment as the flow progressing downstream. From the figure, the end of the jet's potential core is situated between  $x = 0.8$ - $0.9$ m, or  $3.6$ - $4D_h$ , where  $D_h$ , is the hydraulic diameter of the nozzle. It is expected that this length is relatively unchanged with the range of Reynolds numbers proposed here. Distribution of the velocity profiles averaging across the y axis at different spanwise location of the nozzle exit plane at  $x = 0.05$ m is shown in Fig. 21b. From the figure, apart from the left and right edges where mixing layers pertain, the velocity profile across the nozzle exit plane is found to be uniform at an average jet velocity of 21.6m/s. Low velocity variation was demonstrated by the error bars that correspond to the upper and lower velocity limits inside the potential core. The results in Figs. 21a and 21b provide a clear contour of the potential core in which the airfoil can be effectively submerged into for the trailing edge self-noise study.

A TSI 1210-T1.5 miniature hot wire probe with  $3.8\mu\text{m}$  diameter was used to measure the turbulence intensity in the exit jet. The hot wire was heated by a constant-temperature anemometer (TSI IFA300E) with an overheat ratio of 1.8. The

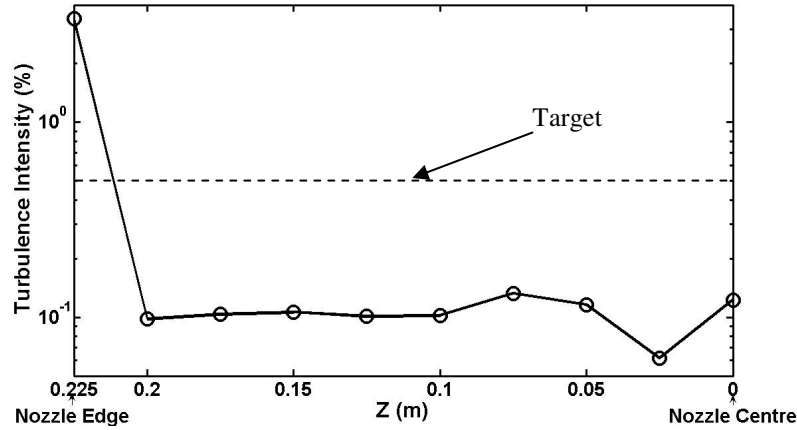


**Fig. 22** Spanwise ( $z$ ) distribution of turbulence intensity of the exit jet at  $60\text{ms}^{-1}$  at  $(x, y) = (0.1, 0)$ .

same computer-controlled traverse system was used to measure at several points from the nozzle edge to the centre in a single run. The signals from the hot wire were sampled at a frequency of 5kHz with a 2.5kHz anti-aliasing filter and the typical sampling time was 5 seconds at each point. Figure 22 shows the distribution of turbulence intensity in  $z$ -axis of the free jet at 60m/s from the nozzle edge ( $z=0.225\text{m}$ ) to the centre ( $z=0$ ). This measurement was performed at 0.1m away from the nozzle exit. Apart from the first point near the edge located within the shear layer, the potential core of the free jet has a typical turbulence intensity of about 0.1%. This distribution is well below the initial target of 0.5%. With such low disturbance level in the free flow, extraneous noise caused by the interaction of the jet turbulence with the aerofoil leading edge will be small.

## 7. Measurements of Aerofoil Trailing Edge Noise

After the open jet wind tunnel was calibrated, a NACA0012 aerofoil was submerged within the potential core of the jet to assess the trailing edge self-noise in relation to the wind tunnel background noise. The aerofoil is 0.15m in chord and 0.45m in span, and was held at zero angle of attack by side plates extended from the nozzle sidewalls. Rough sandpaper was placed near the leading edge of the aerofoil at both of the pressure and suction sides to trip the boundary layers. The radiated noise was measured at 0.35m above the trailing edge, which corresponds to  $90^\circ$  polar angle,  $\theta$ .

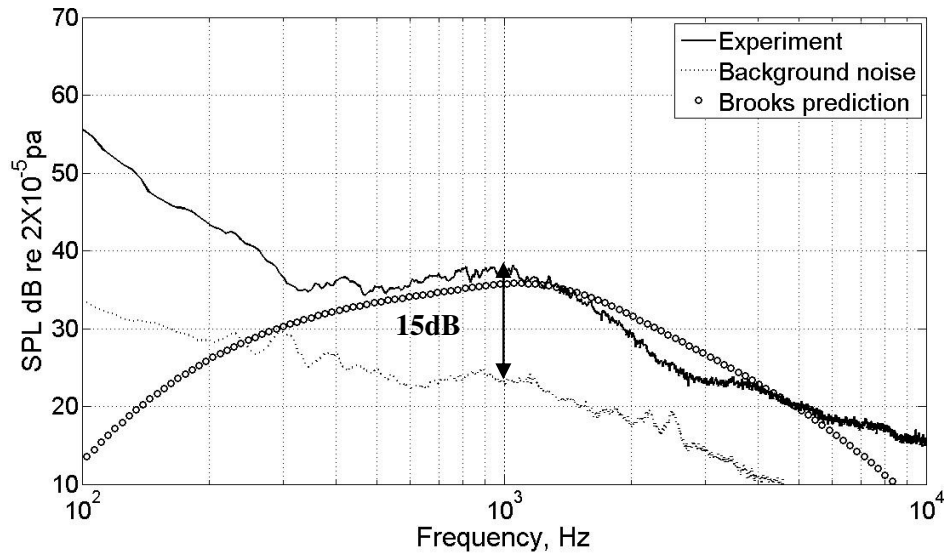


**Fig. 23** Narrowband spectrum of the measured trailing edge noise at 0.35m above the nozzle exit plan, corresponding to polar angle of 90 degree. The relevant spectra for the airfoil noise prediction by Brooks and the facility background noise are also included for comparisons.

At first, the background noise of the open jet wind tunnel was measured under jet velocity of 33.3m/s. The aerofoil was then attached to the sidewalls and the same jet velocity was repeated again. The resultant narrowband noise spectra of these cases were plotted in Fig. 23. Also shown in the figure is the empirical prediction scheme developed by Brooks<sup>6</sup>. Good agreement is observed over the frequency range of 0.5-6kHz. The trailing edge self-noise measurement is seen to be more than 10dB above the background wind tunnel noise and more than 15dB above it at the peak frequency of 1kHz.

## 8. Conclusions

A quiet, high speed and low turbulence open jet blow down wind tunnel has been carefully designed and built in the ISVR, University of Southampton. Situated in a large anechoic chamber, this facility is designed to achieve a maximum Reynolds number of  $1.5 \times 10^6$  based on the hydraulic diameter of the nozzle. This technical report presents the design principle and in-depth discussions for each essential component of the open jet wind tunnel. A unique quiet control valve was identified to minimise the valve noise caused by the large pressure drop. The valve noise present in the flow is further attenuated by a downstream large-scale silencer with absorptive baffles. The amount of transmission loss of this silencer has been

experimentally verified and the result matches the expectation well. For the seemingly short 90°-curved diffuser, several passive flow control devices were attempted with the aim of inhibiting boundary layer separation on the inner-wall. After performing extensive experiments in a scaled-down model of the curved-diffuser, it was determined that three splitter vanes, a honeycomb and woven wire mesh screens with at least  $5.5q$  pressure drop characteristic is the optimum combination. Immediately downstream of these flow control devices a settling chamber was installed to help the flow settling down. In addition, several splitters that were stuffed with sound absorbing materials had been fitted in the settling chamber to further attenuate the residue valve noise and dissipate any upstream boundary layer noises. The final component is a 25:1 *CR* 3D nozzle where air is accelerated and discharged into the atmosphere. Acoustic and aerodynamic evaluations of the open jet wind tunnel were performed after the wind tunnel was commissioned. The results suggested that a low facility noise was achieved and the free jet was aerodynamically clean with low turbulence intensity. Furthermore, the low OASPL characteristic indicates that the present facility is as good as other world-class aeroacoustic and automobile wind tunnels. A benchmark test was performed by submerging a NACA0012 airfoil with boundary layer tripping element in the free jet and the resultant trailing edge self-noise was measured. The high signal-to-noise ratio of the results means that the open jet wind tunnel meets the criteria for trailing edge self-noise measurements that require low background noise and laminar jet to avoid leading edge impingement noise. Although this wind tunnel is originally built for trailing edge self-noise measurement, it can easily be extended to other aeroacoustic applications, which makes it a versatile aeroacoustic research facility.

## 9. Acknowledgements

The work reported in this report is sponsored by the DARP MSTARR in the UK. The authors would like to thank John Coupland of Rolls-Royce for his helpful comments and supports throughout the project. The design and calculation of the primary silencer by Professor Alan Cummings at Hull University are greatly appreciated. The authors would also like to thank Keith Sims, David Edwards,

Jeffrey Andrews and Dennis White in ISVR for their dedicated efforts in designing and fabricating the wind tunnel.

## 10. Nomenclatures

$A_{iFacility}, A_{ISVR}$	Nozzle areas for other wind tunnels and ISVR open jet wind tunnel respectively, $m^2$
$AR$	Area ratio, $W_2/W_1$
$C_{po}$	Non-dimensional total pressure coefficient at diffuse exit plane, $C_{po} = \frac{P_o(y_o, z_o) - P_{ref}}{P_{o,ref} - P_{ref}}$
$CR$	Contraction ratio of the nozzle
$d$	Wire mesh thickness, mm
$D_h$	Hydraulic diameter of the nozzle, m
$K$	Pressure drop coefficient caused by the screens
$L$	Straight diffuser axial length, m
$L_{in}, L_{out}$	Lengths of inner and outer wall arcs of the curved diffuser respectively, m
$N$	Power factor of velocity dependency
OASPL	Overall Sound Pressure Levels, dB or dBA
$P$	Pitch of wire mesh screen, mm
$\overline{p^2}$	Mean square pressure of noise level, $Pa^2$
$P_o(y_o, z_o)$	Total pressure measured at the curved-diffuser exit in $y_o$ - $z_o$ plane, Pa
$P_{o,ref}, P_{ref}$	Reference total and static pressures at 30mm before the curved-diffuser inlet, Pa
$q$	Dynamic pressure, $\frac{1}{2}\rho V^2$ , Pa
$r_{iFacility}, r_{ISVR}$	Distance from the microphone to the centre of the nozzle exit plane for other wind tunnels and ISVR open jet wind tunnel respectively, m
TL	Transmission loss of noise, dB
$U_{dev}$	Deviation of velocity compared with the flow at the outer wall region, see Eq. 1
$U_{outer, Z=0.5}$	Velocity at outer wall at $Z=0.5$ , m/s
$U_{Y, Z=0.5}$	Velocity from outer wall to inner walls at $Z=0.5$ , m/s
$v_p, V$	Exit jet velocity, m/s
$W_1, W_2$	Diffuser widths at inlet and outlet respectively, m
$x, y, z$	Axial, normal and spanwise distances from origin of the nozzle exit, defined in Fig. 16c, m
$y_o, z_o$	Normal and spanwise distances from origin of the $90^\circ$ -curved diffuser exit, defined in Fig. 9a, m
$Y_o$	Normalisation of $y_o$ , $\frac{y_o}{0.195}$ (scale-model) or $\frac{y_o}{1.3}$ (full-size)
$Z_o$	Normalisation of $z_o$ , $\frac{z_o}{0.195}$ (scale-model) or $\frac{z_o}{1.3}$ (full-size)
$\beta$	Screen porosity, defined in Fig. 13
$\Delta\phi$	Curved diffuser turning angle, degree, see Fig. 7b

$\Delta p$	Static pressure drop across mesh screens, Pa
$\rho$	Density of air, kg/m <sup>3</sup>
$\theta$	Polar angle from the jet axis, deg
$\zeta$	Diffuser divergence angle, deg

## 11. References

1. Amiet, R., 1976, "Noise due to Turbulent Flow Past a Trailing Edge", *JSV*, **47**, 387-393
2. Howe, M. S., 1999, "Trailing Edge Noise at Low Mach Numbers", *JSV*, **225**(2), 211-238
3. Oberai, A. A., Roknaldin, F. and Hughes, T. J. R., 2002, "Computation of Trailing-Edge Noise due to Turbulent Flow Over an Airfoil", *AIAA J.*, **40**, 2206-2216
4. Wang, M. and Moin, P., 2000, "Computation of Trailing-Edge Flow and Noise Using Large-Eddy Simulation", *AIAA J.*, **38**, 2201-2209
5. Sandberg, R. D., Sandham, N. D. and Joseph, P. F., 2007, "Direct Numerical Simulations of Trailing-Edge Noise Generated by Boundary-Layer Instabilities", *JSV*, **304**(3-5), 677-690
6. Brooks, T. F., Pope, D. S. and Marcolini, M. A., 1989, "Airfoil Self-Noise and Prediction", Tech. rep., NASA Reference Publication 1218
7. Roger, M. and Moreau, S., 2004, "Broadband Self-Noise from Loaded Fan Blades", *AIAA J.*, **42**(3), 536-544
8. Ura, H., Yokokawa, Y. and Ito, T., 2007, "Experimental Study of Trailing Edge Noise in Low-Speed Wind Tunnel", Collection of Technical Papers - 45<sup>th</sup> *AIAA Aerospace Sciences Meeting*, **18**, 12536-12549
9. Duell, E., Walter, J., Arnette, S. and Yen, J., 2002, "Recent Advances in Large-Scale Aeroacoustic Wind Tunnels", 8<sup>th</sup> *AIAA/CEAS Aeroacoustic Conference and Exhibit*, Breckenridge, Colorado, AIAA Paper 2002-2503
10. Mathew, J., Bahr, C., Sheplak, M., Carrol, B. and Cattafesta, L. N., 2005, "Characterization of an Anechoic Wind Tunnel Facility", Proceedings of ASME, *IMECE*, Orlando, Florida, IMECE2005-81737
11. Leclercq, D., Doolan, C. and Reichl, J., 2007, "Development and Validation of a Small-Scale Anechoic Wind Tunnel", 14<sup>th</sup> *International Congress on Sound and Vibration*, Cairns, Australia
12. Coupland, J. (Rolls-Royce Plc), Private communication
13. Cummings, A., 1978, "The Attenuation of Lined Plenum Chambers in Ducts: I. Theoretical Models", *JSV*, **61**, 347-373
14. Kline, S. J. and Johnston, J. P., 1986, "Diffusers: Flow, Design, and Performance Prediction, Part 1: Diffuser- Flow Phenomena and Design", *Advanced topics in turbomachinery technology* (PLS-2) (D. Japikse, ed.), Concepts ETI, Inc.
15. Sagi, C. J. and Johnston, J. P., 1967, "The Design and Performance of Two-Dimensional, Curved Diffusers", *Trans. ASME, J. Basic Engng*, **89**, 715-731
16. Chong, T. P., Joseph, P. F. and Davies, P. O. A. L., 2008, "A Parametric Study of Passive Flow Control for a Short, High Area Ratio 90 Degree Curved Diffuser", *Trans. ASME, J. Fluids Engng*, accepted for publication.
17. Pinker, R. A. and Herbert, M. V., 1967, "Pressure Loss Associated with Compressible Flow through Square-Mesh Wire Gauzes", *J. Mech. Engng. Sci.*, **9** (1), 11-23
18. Bradshaw, P., 1964, "Wind Tunnel Screens: Flow Instability and Its Effect on Aerofoil Boundary Layers", *Journal of Royal Aeronautical Society*, **68**, pp. 168
19. Kurze, U., 1969, "Sound Propagation in a Duct of Periodic Wall-Structure," *Acustica*, **21**(2), 74-85
20. Abramovich, G. N., 1963, "The Theory of Turbulent Jets", The M.I.T. Press, Cambridge, Massachusetts